Nanoscale

Accepted Manuscript

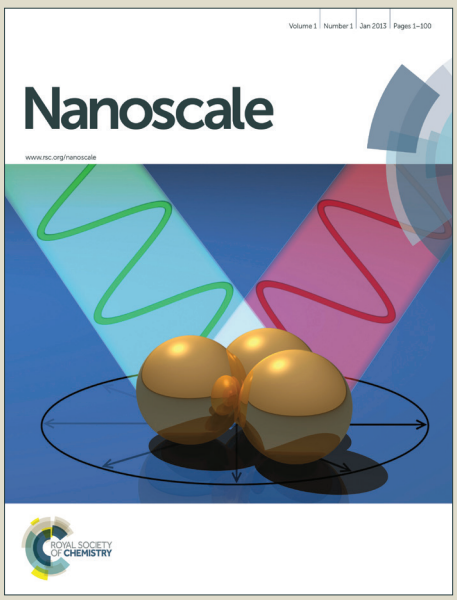

ROYAL SOCIETY OF CHEMISTRY

www.rsc.org/nanoscale

Nanoscale

RSCPublishing

ARTICLE

Self-assembled Gold Coating Enhances X-ray Imaging of Alginate Microcapsules

Cite this: DOI: 10.1039/xoxxoooooox

Fengxiang Qie,[a,b] Alberto Astolfo,[c,d] Malsha Wickramaratna,[b] Martin Behe,[e] Margaret D. M. Evans,[f] Timothy C. Hughes,*[b] Xiaojuan Hao,*[b] and Tianwei Tan*[a]

Received ooth January 2012,
Accepted ooth January 2012

DOI: 10.1039/xoxxoooooox

www.rsc.org/

Therapeutic biomolecules produced from cells encapsulated within alginate microcapsules (MCs) offers a potential treatment for a number of diseases. However the fate of such MCs once implanted into the body is difficult to establish. Labelling the MCs with medical imaging contrast agents may aid their detection and give researchers the ability to track them over time thus aiding the development of such cellular therapies. Here we report the preparation of MCs with a self-assembled gold nanoparticle (AuNPs) coating which results in distinctive contrast and enables them to be readily identified using a conventional small animal X-ray micro-CT scanner. Cationic Reversible Addition-Fragmentation chain Transfer (RAFT) homopolymer modified AuNPs (PAuNPs) were coated onto the surface of negatively charged alginate MCs resulting in hybrids which possessed low cytotoxicity and high mechanical stability *in vitro*. As a result of their high localized Au concentration, the hybrid MCs exhibited a distinctive bright circular ring even with a low X-ray dose and rapid scanning in *post-mortem* imaging experiments facilitating their positive identification and potentially enabling them to be used for *in vivo* tracking experiments over multiple time-points.

Introduction

Alginate is a naturally occurring anionic polymer typically isolated from seaweed, that has been extensively investigated for many biomedical applications, due to its low toxicity, relatively low cost, and mild gelation by addition of divalent cations such as Ca^{2+} and Ba^{2+}.[1] Alginate is currently used as wound dressing material for the treatment of acute or chronic wounds.[2] It also plays a crucial part in the delivery of bioactive agents such as small molecule drugs[3-5] and proteins.[6-8] Most importantly, crosslinked alginate hydrogels have proven to be the most advantageous for cell encapsulation,[1] particularly in encapsulating insulin producing cells (islets) for diabetes treatment.[9]

Islet transplantation is an attractive treatment for patients with type I diabetes[10] but success has been limited, partially as a result of the requirement for cytotoxic immunosuppressive regiments.[11-14] To avoid immunosuppressive therapy, microencapsulation has been proposed as a method of protecting transplanted cells from the host's immune system.[15-17] By surrounding insulin producing cells with a thin semi-porous alginate membrane *i.e.* encapsulating islets in alginate microcapsules (MCs) that are selectively permeable to insulin and metabolites but impermeable to antibodies, microencapsulation provides a promising solution to isolate cells from the host's immune system while preserving cell function and integrity.[18-20] However, it is difficult to determine the position, integrity, and fate of such MCs once implanted in the body due to their small size and difficulties in explanting them. Labelling MCs by with medical imaging contrast agents may aid the researcher's ability to track such MCs within the body and thereby aid the development of such cellular therapies.

A variety of traditional imaging modalities, which are both clinically used and widely available, have been proposed to track the position and integrity of MCs. The Bulte group has previously shown the possibility of tracking MCs with various contrast agents, such as the radio-opaque agents barium or bismuth sulfate[21-23] and gold[24, 25] for detection by CT/X-ray modalities, superparamagnetic iron oxide (SPIO) for detection by ^{1}H MRI[14, 25-28] or perfluorocarbon (PFC) emulsions for multimodal detection by ^{19}F MRI, X-ray, and ultrasonic (US) imaging.[29] In general, for long term imaging, it is desirable to have contrast agents which have a long term stability, and are non-toxic to cells thus do not affect cell function. Colloidal gold nanoparticles (AuNPs) have become an important option as medical imaging contrast agents due to their high X-ray absorption coefficient (at 30 keV the absorption coefficients of gold and iodine are 27.5 cm^2/g and 8.6 cm^2/g, respectively),[30] low cytotoxicity, as well as their non-susceptibility to photobleaching[31] or chemical/thermal denaturation.[32, 33] Taking into account of the advantages and disadvantages of the various contrast agents, we were interested in investigating AuNPs as contrast agents for X-ray imaging of alginate MCs. X-ray based technique exhibits a number of advantages over other established imaging methods, such as its extremely high spatial and temporal resolution, high penetration depth, which allows us to see and quantify small clusters of marked cells in *ex vivo* animals in detail at multiple anatomical locations.[34] Astolfo *et al.* demonstrated the ability to perform cell tracking using X-ray CT combined with AuNPs on *in vivo* samples using a malignant cell line[35] and the possibility to obtain single cell resolution using a conventional microfocus X-ray tube on *ex vivo* samples.[36] Shi *et al.* reported synthesis of acetylated dendrimer-entrapped AuNPs for *in vivo* CT imaging of cancer cells[37] and PEGylated dendrimer-entrapped AuNPs for blood pool, and xenograft tumors imaging.[38] Ahn *et al.* reported the incorporation of surface-modified AuNPs into human red blood cells as optimized flow tracers generating effectively enhanced dynamic X-ray imaging to observe the dynamic motions of blood flows.[39] In spite of potential biomedical applications of

functionalized AuNPs, there are only a few reports available on toxicity, visibility, and resolution of X-ray imaging of MCs using AuNPs.[24, 25, 29, 40] One of the challenges in X-ray imaging is optimization of the Au concentration used. While a higher Au concentration allows the contrast agent to be easily distinguished from surrounding tissues, it is also more likely to be cytotoxic. Moreover, at a lower Au concentration it can be difficult to distinguish the MCs from reconstruction artifacts or other anatomic details in the image. Previous studies have shown that blending AuNPs into alginate MCs enabled them to be imaged using conventional CT machines.[25, 41, 42] However, at lower Au concentrations it can be difficult to accurately segment the labeled capsules. More recently, macroscale contrast agents with distinctive shapes have been proposed to counter the issue of detection and positive identification at low contrast levels.[43, 44] However the use of unnatural and distinctive shapes to aid the identification of labeled MCs has not been previously reported.

In this work, we have developed a novel fabrication method to improve the X-ray opacity of alginate MCs and thus enhance their contrast and potentially enable them to be tracked *in vivo*. Three different homopolymers were synthesized *via* Reversible Addition-Fragmentation chain Transfer (RAFT) polymerization, which were coated onto AuNPs *via* either electrostatic interaction or chemical binding (*via* thiol groups). Polymer-AuNPs (PAuNPs) were then electrostatically coated outside of alginate MCs to form a layer of gold on the surface. The fabricated PAuNPs-MCs were then used for X-ray imaging to evaluate MCs visibility. To the best of our knowledge, this is the first report using PAuNPs to decorate the outside of the alginate MCs effectively as a thin layer of gold coating to form stable gold labeled MCs enabling them to be more readily identified using X-ray imaging.

Results and Discussion

Synthesis of Homopolymers

The cationic 2-(methacryloyloxy)ethyl trimethylammonium chloride (METAC) polymer was selected to modify the AuNPs in order to enable the electrostatic interaction of AuNPs with the negatively charged alginate MCs. As an alternative approach, the neutral poly(ethylene glycol) methacrylate (PEGMA) polymer was also selected to coat the AuNPs as it is well known to be non-immunogenic, non-antigenic, and low protein fouling.[45, 46] The two different homopolymers of METAC and PEGMA were synthesized using a dithioester RAFT agent with 2,2'-azobis-(isobutyronitrile) (AIBN) as an initiator, as shown in Scheme 1. In addition to controlling the molecular weight and polydispersity, RAFT polymerization enables the generation of polymers with thiol end groups upon RAFT end group removal by aminolysis, which can be used to immobilize the polymer on the gold surface through stable Au-S bonds.[47]

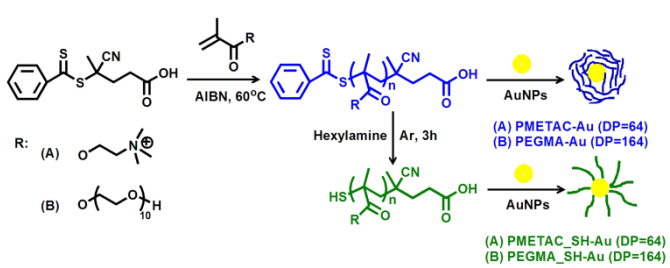

Scheme 1 Polymers synthesis and modification of AuNPs.

The polymerizations were terminated at a high monomer conversion (METAC, 94.1%; PEGMA, 90.7%). ^{1}H NMR analysis revealed the presence of the RAFT end groups with the signals between δ 7-8 ppm assigned to the RAFT phenyl group (Figures S1a, S2a). Corresponding thiol-group capped polymers (PMETAC_SH, PEGMA_SH) were generated by aminolysis reaction and investigated by ^{1}H NMR which confirmed the disappearance of the RAFT end group (Figures S1b, S2b).

Table 1 Molecular weight (M_n) of homopolymers

Samples	DP		Molecular weight (g/mol)		PDI
	Target	NMR	NMR M_n	GPC M_n	
PMETAC	50	64	13590	4553	1.13
PMETAC-SH	50	64	13470	4302	1.15
PEGMA	200	164	86540	66540	3.33
PEGMA-SH	200	164	86420	79600	3.82

The molecular weights of prepared homopolymers measured by gel permeation chromatography (GPC) and nuclear magnetic resonance (NMR) spectroscopy are summarized in Table 1. GPC results showed that the number-average molecular weights (M_n) of cationic polymers (PMETAC and PMETAC_SH) were 4550 g/mol and 4300 g/mol, respectively, and both polymers had narrow polydispersities (PDIs below 1.2). The difference between GPC and NMR results may come from the calibration curve used in the GPC analysis (using polyethylene oxide (PEO) standards). However, there is a good agreement between the NMR and GPC molecular weights for PEGMA and PEGMA_SH polymers. A broader polydispersity index (PDI) was observed for PEGMA polymers, which may be due to the polydispersity of PEGMA monomer and was consistent with the results from other PEG polymerizations.[48, 49]

Synthesis of AuNPs

AuNPs of 60 nm in diameter were synthesized *via* the established citrate reduction method[50] and characterized by UV-Visible spectrophotometer (Figure S3a), dynamic light scattering (DLS) (Figure S3b), and transmission electron microscopy (TEM) (Figure 1a). The diameter of the PAuNPs as determined by UV-Visble measurement[51] was in a good agreement with DLS analysis and TEM observation.

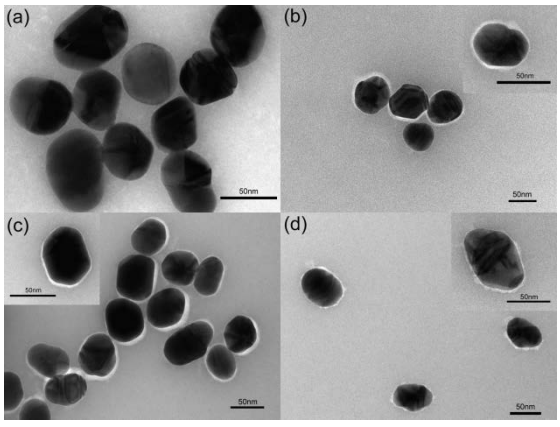

Fig. 1 TEM images with negative staining: unmodified AuNPs (a); AuNPs coated with PMETAC (b); PMETAC_SH (c); and PEGMA_SH (d).

Synthesis of PAuNPs and Characterization

Surface modification of AuNPs is required to prevent particle aggregation.[52, 53] In this work, RAFT polymers were designed to interact with AuNPs *via* electrostatic interaction and/or gold-sulfur interactions *via* the thiol end groups generated by RAFT

end group removal.[47] A red shift in gold surface plasmon resonance peak confirmed the successful coating of AuNPs with PMETAC, PMETAC_SH, and PEGMA_SH, respectively (Figure S3a).

The hydrodynamic diameters measured by DLS are shown in Figure S3b and Table S1. The results confirmed an increase in hydrodynamic volume of these AuNPs after modification with various polymers. The difference in particle size between the samples may be due to the difference in polymer chain orientation that arises from the different polymer chain lengths and modes of interactions between the polymers and the AuNPs. Presumably, PMETAC wraps around the AuNPs as it can bind to AuNPs *via* electrostatic interaction with the positively charged monomer units (Scheme 1). Whereas PMETAC_SH may bind to the AuNP *via* the thiol end group, thus may be able to stretch out from the AuNPs and occupy more space. In addition, the diameter of PEGMA_SH-Au was larger presumably due to the increased degree of polymerization (DP) of the polymer used, leading to an increased thickness of the PEGMA_SH layer. PEGMA RAFT polymer failed to bind to the AuNPs presumably because both the dithoester group and the polymer did not have sufficient interaction with the AuNPs. In contrast, hydrophobic polymers containing trithiocarbonate RAFT end groups are known to form strong interactions with AuNPs.[54, 55]

The functionalization of AuNPs with RAFT polymers was also followed by zeta potential measurements. As shown in Figure S3c the zeta potential of nanoparticles changed following the addition of various polymers indicating the change in surface charge and thus successful surface modification owing to different interaction mechanisms and polymer charge.

The presence of the polymer layer on the gold surface was confirmed by TEM with the assistance of negative staining.[56] The addition of a negative stain enhances the contrast between AuNPs and the polymer layer in TEM analysis and the images show a clear white corona around the AuNPs strongly suggesting the presence of a polymer layer (Figure 1).

The grafting density of different polymers can be determined from the mass loss (wt%) in TGA measurement from 100 ºC to 650 ºC (Figure S4 and Table 2).

Table 2 Grafting density of different polymers on AuNPs

Polymer	Mass loss (wt%)[a]	Grafting density (chains/nm^2)[b]
PMETAC	1.30%	0.099
PMETAC_SH	1.10%	0.085
PEGMA_SH	8.00%	0.403

[a] Mass loss (wt%) was determined by TGA;

[b] Grafting density was calculated by the following equation:[57]

Grafting density = $[(\text{mass loss}/M_n^{\text{Polymer}}) \times N_a]/[m^{\text{AuNPs}} \times S^{\text{AuNPs}}]$

Where mass loss, M_n^{Polymer}, N_a, m^{AuNPs}, S^{AuNPs} correspond to the mass of the polymer grafted determined by TGA (Figure S3), number-average molecular weight of the polymer, Avogadro's number, mass of AuNPs used for the TGA analysis and the surface area of unmodified AuNPs.

Synthesis of PAuNPs-MCs

AuNPs modified with three different polymers (PAuNPs), PMETAC-Au, PMETAC_SH-Au, and PEGMA_SH-Au, were coated onto pre-formed alginate MCs (Scheme 2). The interaction between PAuNPs and MCs could be visually observed simply by mixing the two components together and watching the resulting change in colour. In a control experiment, when the colourless MCs were mixed with unmodified AuNPs (Figure 2b) the AuNPs solution remained red purple colour and the MCs remained colourless, indicating no interaction between AuNPs and MCs. Likewise, no colour change was observed when PEGMA_SH-Au were mixed with MCs indicating no interaction between the two, however PEGMA_SH-Au could be incorporated into MCs *via* the blending method as reported previously.[42] PEGMA_SH-Au could not bind to the pre-formed MCs surfaces presumably due to the neutral nature of the polymer and thus the lack of a suitable interaction. However, in contrast, when MCs were mixed with PMETAC-Au and PMETAC_SH-Au, MCs rapidly changed to dark gold colour and the solution became colourless simultaneously, indicating a fast, essentially quantitative electrostatic attraction of the polymer modified AuNPs onto MCs due to a strong electrostatic interaction (Figure 2c for PMETAC-Au-MCs).

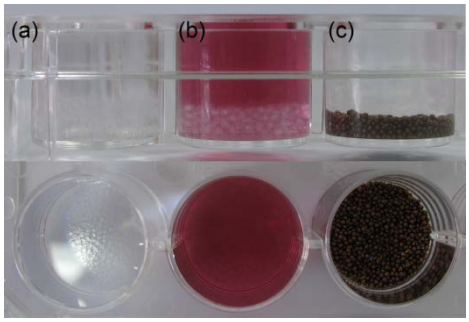

Fig. 2 Pictures of (a) alginate MCs; (b) mixture of alginate MCs and unmodified AuNPs solution; (c) mixture of alginate MCs and PMETAC-Au solution.

Figure S5 shows scanning electron microscopy (SEM) images of MCs and PAuNPs-MCs surfaces and cross-section at a higher magnification. The synthesized alginate MCs were visibly spherical in shape and had a regular porous surface (Figure S5A). PAuNPs were uniformly distributed and entirely covered the MCs surface (Figure S5B). Energy dispersive spectroscopy (EDS) analysis (Figure S6) confirmed the presence of gold evenly distributed over the surface of MCs (PMETAC_SH-Au-MCs), consistent with SEM observation.

In order to further confirm that the PAuNPs were only on the surface, SEM analysis was performed on cross-section of dried resin embedded MCs (Figure S7). The internal alginate structure can be clearly differentiated from PMETAC-Au coating (about 4 µm thick). EDS also confirmed that gold was present only in the coating (spots 12, 13) and not within the internal structure (spots 14, 15) (Figure S7).

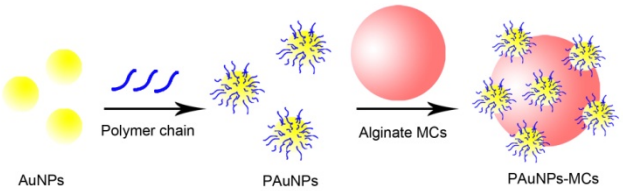

Scheme 2 Fabrication method of PAuNPs-MCs.

In Vitro Cytotoxicity of PAuNPs-MCs

To evaluate cytotoxicity of PAuNPs-MCs, L929 cells were exposed to PAuNPs coated alginate discs and compared to uncoated alginate discs in a direct contact cytotoxicity assay which also included the following control samples: serum-free medium (SFM; positive control), 5% phosphate buffer saline (PBS) (positive control), and 5% dimethyl sulfoxide (DMSO) (negative control). Typically, a material is considered cytotoxic when the cell viability is below 70% of the value for SFM control. Figure 3 clearly shows that cells incubated in direct contact with the PMETAC_SH-Au (Au conc. 4.7 g/L) coated

discs (polymer containing thiol group) had a similar cell viability to the control alginate discs while the PMETAC-Au (Au conc. 4.7 g/L) coated discs (polymer containing RAFT end group) exhibited a slightly lower level of cell viability. Interestingly, the PMETAC was less cytotoxic with the RAFT end group removed which was consistent with the cytotoxicity results of other RAFT polymers.[58] Therefore, it can be concluded that the obtained PMETAC_SH-Au-MCs exhibited low cytotoxicity even at a high Au concentration (4.7 g/L), showing their suitability for biomedical applications.

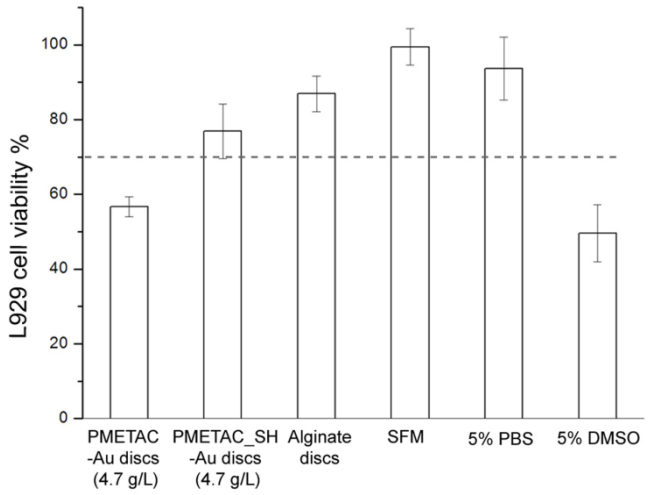

Fig. 3 Cytotoxicity of alginate discs coated with PMETAC-Au (4.7 g/L) and PMETAC_SH-Au (4.7 g/L) in comparison with alginate discs and control samples SFM, 5% PBS, and 5% DMSO.

Stability of PAuNPs-MCs

To ensure that the MCs can be tracked over time, it is essential that the AuNPs remain bound to the MCs. The mechanical stability of PAuNPs-MCs in saline shaken at 110 rpm at 37 ºC was monitored by visual observation of MCs and UV-Visible spectroscopy measurement of the medium. Visual inspection under optical microscope showed that the MCs remained intact and undamaged after 2 months of shaking at 37 ºC. Moreover, the labeled MCs remained intact and undamaged after steam autoclaving (Figure S8). In all cases, UV-Visible spectroscopy measurement of the medium revealed that the Au concentration in the physiological (0.9 w/v%) saline solution containing the MCs was essentially undetectable (less than the detectable limit of about 0.8 mg/L), further confirming the good mechanical stability of the PAuNPs coating (Figure S9), indicating that the PAuNPs layer bound tightly on MCs.

X-ray Attenuation Property of PAuNPs-MCs

The reconstructed CT data of the MCs was used to evaluate the linear attenuation coefficient (μ) of the labeled MCs. The gray scale data calibration was performed using the signals from air, ethanol, water, and a 10% iodine solution. The signals from 20 MCs per sample were measured. The profiles were taken on about the middle of the MCs.

The measurements were performed using a 25 keV monochromatic X-ray beam in order to evaluate the contrast for small animal imaging. Between 80 and 15 keV the gold linear attenuation coefficient increased as energy decreased. Thus, a lower energy is preferable to increase the MCs visibility. However, lower energies are more absorbed / attenuated by the matter with the consequence of increasing the X-ray dose delivered. For the same reason, at lower energies the X-ray penetration depth decreases yielding imaging on small animals impracticable at energies lower than 20 keV. It is important to generate a high contrast between the MCs and the surrounding tissue that is not lost by a high image noise (typically high for low dose CT). As examples, the theoretical μ of soft and adipose tissues are 0.546 cm^{-1} and 0.368 cm^{-1} at 25 keV.[59] The coating method used here results in a higher localized Au concentration which results in a significant increase of μ compared to that reported for comparable AuNP blended MCs (c.f. 1.5 *vs* 0.87 cm^{-1} at 25 keV with Au conc. 3.08 g/L, respectively),[42] as shown in Figure 4. In addition, our best AuNP labelled MCs had significantly higher μ than the unlabelled MCs, 1.74 *vs* 0.51 cm^{-1}, respectively.

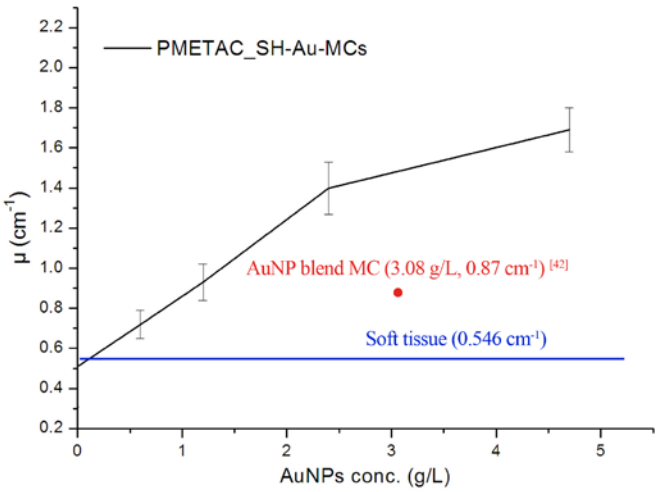

Fig. 4 Attenuation coefficients measured with monochromatic synchrotron radiation at 25 keV.

Application of PAuNPs-MCs for X-ray Imaging

We explored the feasibility of using PAuNPs-MCs for X-ray imaging utilizing a *post-mortem* animal model. PMETAC_SH-Au-MCs were chosen as the lead candidate for X-ray imaging studies based on the outcome of the *in vitro* cytotoxicity results. After injection of a saline solution containing PMETAC_SH-Au-MCs (about 20 MCs per 100 µL) into each mouse through abdominal cavity, the cadavers were then used for the tomographic scan. Preliminary imaging was performed using monochromatic synchrotron radiation. Labeled MCs implanted within wiener rats could be readily observed (Figure S10). Obviously, the labeled MCs were much easier to be visualized compared to the unlabeled MCs in which no MCs could be positively identified (Figure S11). However, for this technique to be more widely applied there needs to be sufficient contrast to overcome the inherent noise for use in conventional polychromatic small animal CT machines at a low X-ray dose.

Imaging in a small animal CT scanner at a low X-ray dose also produced images where the labeled capsules could be readily distinguished from the surrounding tissue even with rapid acquisitions (only about 5 minutes) (Figure 5a-c). In the CT images, soft tissues including muscles and blood vessels show a lower X-ray attenuation similar to water; therefore they appear gray. The air bubbles due to the early stage of the animal decomposition result in black regions were also visible in the 3D rendering in Figure 5e. In contrast, bones appear white

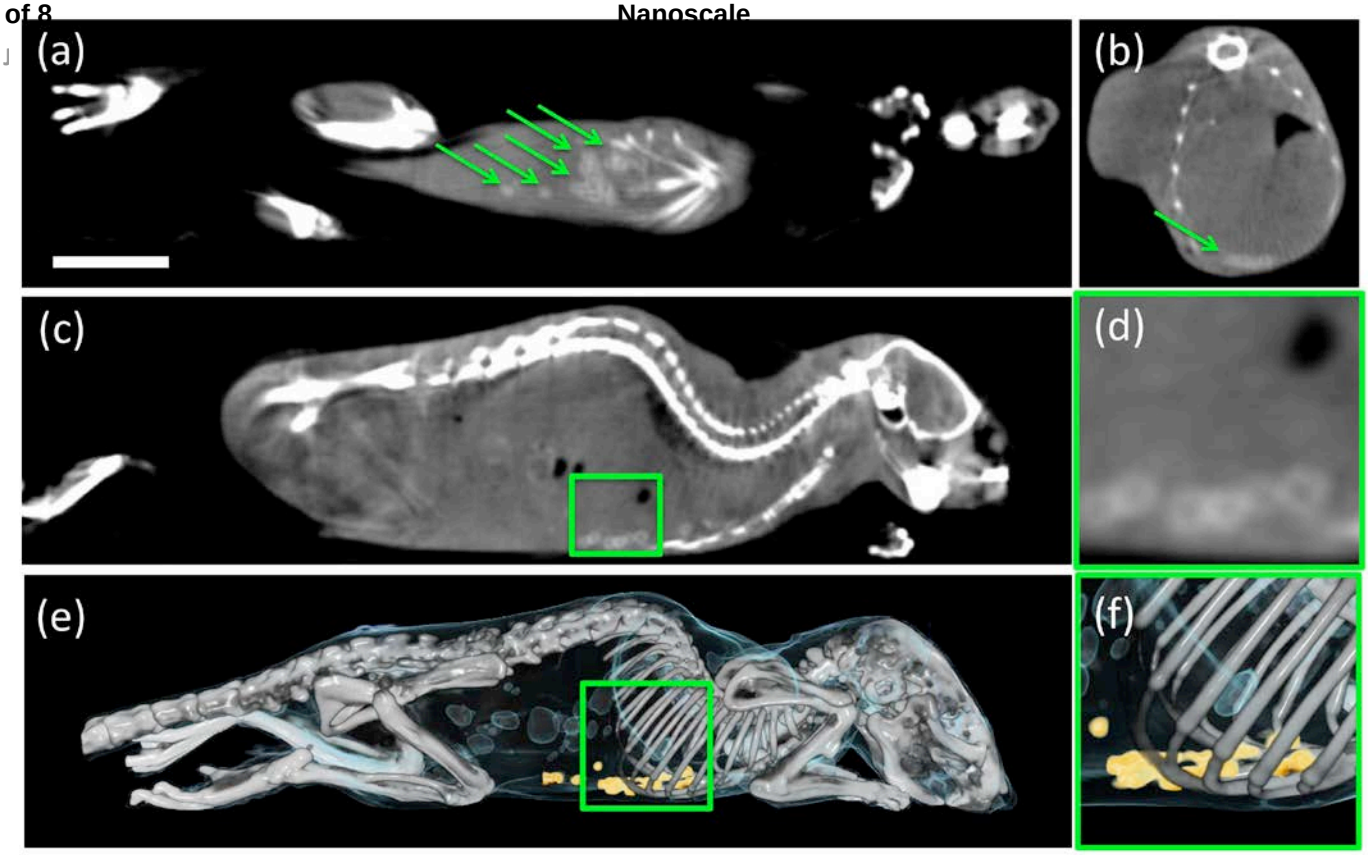

Fig. 5 X-ray micro-CT reconstructed data of a mouse injected with PMETAC_SH-Au-MCs (4.7 g/L) (CTDI 28 mGy) in coronal (a) transverse (b) and sagittal (c) views with the magnification of the detail in the square shown in (d). Arrows indicate the MCs. 3D rendering of the same mouse with the MCs artificially coloured in yellow (e) and the detail in the square magnified in (f). Scale bar 1 cm.

to their higher density and atomic number resulting in a stronger X-ray attenuation, as exemplified by the mouse's spondyle in our case. The existence of PMETAC_SH-Au-MCs within the parenchyma can be visualized in CT image because of their higher attenuation coefficient compared to soft tissue (Figure 5). As expected, the MCs prepared with the highest Au concentration provided the best contrast on X-ray imaging. Owning to the reduced cytotoxicity of MCs coated by PAuNPs without RAFT end groups, a higher loading of PAuNPs could be used compared to our previous report (4.7 vs. 3.75 g/L, respectively),[42] in which we used same RAFT polymer but did not remove the RAFT end groups. Due to differences in the way the data is presented in different publications, it is difficult to make accurate imaging performance comparisons between this work and earlier reports. The use of AuNPs offers the advantage of lower toxicity over $BaSO_4$.[21] In addition, the imaging performance of MCs reported in current study have comparable imaging performance to the best AuNPs imaging previously reported [24, 25] and the fabrication process is simpler compared to the more complex capsule systems.[25] Moreover, at the energy of 25 keV, the attenuation coefficient μ increased to 1.74 cm^{-1} compared to the best results reported (0.87 cm^{-1}).[42] We stress this result because from the imaging point of view a higher Au concentration is preferable. This is because the signal to noise ratio (SNR) is higher (because of a higher signal) so the noise could be increased if necessary. A higher image noise is a consequence of an X-ray dose reduction. This means that higher contrasts permit further reduction of X-ray dose at a constant SNR. Furthermore, the characteristic signal of the MCs (the white circular ring seen in Figures 5c,d) makes it easier to distinguish the MCs from other higher density anatomic details. 3D rendering of X-ray CT images of the MCs can also be quickly performed as shown in Figures 5e,f. The high contrast permitted correct 3D visualization of a single MC using a low dose CT with quick data acquisition (about 5 minutes). In principle, this allows the position of the MCs to be tracked during a longitudinal experiment with high precision.

Experimental

Chemicals: Gold(III) chloride trihydrate ($HAuCl_4$; 99.9%) was purchased from Sigma-Aldrich (Australia) and tri-sodium citrate ($Na_3C_6H_5O_7 \cdot 2H_2O$) was purchased from Ajax Finechem. Monomer poly(ethylene glycol) methacrylate (PEGMA; MW526) was purchased from Sigma-Aldrich (Australia) with inhibitor removed by passing it through a column packed with quaternary ammonium anion-exchanged resin (Aldrich; USA) prior to use. 2-(Methacryloyloxy)ethyl trimethylammonium chloride (METAC; 75%) was purchased from Sigma-Aldrich (Australia) and was purified by precipitation into acetone before use. AIBN was purchased from Sigma-Aldrich (Australia) and was recrystallized twice from ethanol prior to use and then stored at -20 ºC. RAFT agent 4-cyano-4-(thiobenzoylthio)pentanoic acid (CTA, 97%) was purchased from Strem Chemicals (Australia) and used as received. Barium chloride, sodium chloride, diethyl ether, methanol, and ethanol were purchased from Merck. 0.9% Sodium chloride was supplied by Baxter. Pronova alginate was supplied by Novo Matrix. Water was purified with a Millipore Milli-Q system. $BaCl_2$ precipitation bath for crosslinking alginate MCs was prepared by adding $BaCl_2$ (4.89 g), 3-(*N*-morpholino) propane sulfonic acid (2.093 g), and NaCl (6.43 g) to 1 L Milli-Q water followed by stirring until all components were dissolved. All other reagents were used without further purification. PMETAC was prepared as previously reported.[60]

Polymer synthesis

Homopolymerization of PEGMA *via* RAFT process. The polymerization of PEGMA was conducted with the ratio of [PEGMA]/[CTA]/[AIBN] = 200/1/2. PEGMA (5.00 g, 9.51 mmol), CTA (0.0133 g, 0.0476 mmol), AIBN (0.0156 g, 0.0951 mmol), and MeOH (50 mL) were mixed and transferred to a Schlenk vessel, equipped with a stirrer bar. The solution was degassed *via* freeze-pump-thaw for 4 cycles prior to polymerization. Mixture was then placed in a 60 ºC oil bath for 24 h. After the reaction, the vessel tap was opened to let oxygen

in to terminate the reaction. A small amount of reaction mixture was taken for ^{1}H NMR analysis to determine the conversion of monomer (90.7%), which was calculated as 1 minus the ratio of the integration of unreacted monomer double bond (δ 6 ppm) to half the integration of oxymethylene peak (δ 4.16 ppm) which contains both monomer and polymer. The polymer was purified by precipitating into diethyl ether three times. The product was dried in vacuum oven to yield an orange oil (3.37 g, 67.4% yield). The ^{1}H NMR was measured on purified polymer to calculate the degree of polymerization (DP = 164) based on RAFT end group analysis.

Synthesis of polymers containing thiol end groups (PMETAC_SH, PEGMA_SH). RAFT end groups were cleaved off by aminolysis reaction to produce corresponding thiol capped polymers. In detail, METAC or PEGMA polymers (8.31×10^{-6} mol) prepared by RAFT polymerization were dissolved in methanol (10 mL) separately and hexylamine (33 µL) was added under argon at room temperature. The mixture was stirred for 3 h until the pink (or orange) color disappeared. The resulting PMETAC_SH or PEGMA_SH were purified by precipitating into acetone and diethyl ether, respectively. ^{1}H NMR was conducted to ensure the purity of thiol group capped polymers.

Synthesis of AuNPs and their surface modification with polymers. AuNPs with an average diameter of 60 nm were prepared through a citrate-reduction method following literature.[50] AuNPs were modified with a polymer (0.3 mg polymer/mL AuNPs solution) for 30 min before being isolated by centrifugation and removal of the supernatant followed by washing with water (3 times). The concentrated PAuNPs solution was serially diluted in Milli-Q water to a desired concentration prior to use.

Synthesis of alginate MCs and discs. Alginate MCs (average diameter of 500 µm) were prepared by passing 2.2% alginate solution through two-channel air jet droplet maker at 1 mL/min with an air flow rate of 5 L/min. The resulting droplets were crosslinked for 3 min in the $BaCl_2$ precipitation bath positioned 10 cm below the air jet droplet maker. Alginate discs (diameter of 9 mm) were prepared by casting 2.2% alginate solution into the lid wells of a 96 well cell culture plate. After air drying, the discs were crosslinked with $BaCl_2$ solution for 3 min. The generated MCs or discs were washed three times with 0.9 w/v% NaCl to remove residue $BaCl_2$ and stored in saline solution before use.

Fabrication of gold-loaded alginate MCs and discs. The fabrication was performed by transferring 1 mL MCs to 1 mL of PAuNPs solution of various concentrations (4.7, 2.4, 1.2, 0.6 g/L) and then the mixture was put on a shaker (180 rpm) for 30 min, resulting in the formation of PAuNPs coated MCs with PAuNPs loading of about 0.08 to 0.6 µg/MC (estimation in Supplementary Information Section). Three washes were then performed with 0.9 w/v% NaCl solution to remove residue PAuNPs. PAuNPs coated alginate discs were prepared by the same method.

Polymer characterization. NMR analysis of synthesized polymers was performed with a Bruker Av 400 NMR spectrometer. ^{1}H NMR spectra were recorded in deuterium water (D_2O). GPC analysis of the PEGMA and METAC polymers were performed as previously reported.[60]

AuNPs and PAuNPs characterization. Particle size distribution and zeta potential of PAuNPs were measured at 25 ºC in standard disposable cuvettes using a Zeta Sizer-Nano instrument (Malvern, UK). The average of five measurements was reported. The UV-Visible spectra of PAuNPs were measured using a Cary 50 Bio UV-Visible spectrophotometer (Varian Co., USA) at room temperature. The size and concentration of PAuNPs were determined using the method of Haiss *et al.*[51] The morphology and size of PAuNPs were examined by TEM as previously reported.[56] Thermal gravimetric analysis (TGA) of PAuNPs was performed using a Mettler Toledo SDTA/TGA 851e with a heating rate of 10 ºC/min from 100 ºC to 650 ºC. An isotherm at 100 ºC was first maintained for 20 min to eliminate water. The weight loss was calculated from the difference between the weights at 100 ºC and at 650 ºC.

Microcapsules characterization. Iridium coated (Polaron SC5750 sputter coater) dried MCs were imaged using SEM (Philips XL30 Field Emission SEM) at an accelerating voltage of 5 kV. The EDS X-ray analysis (Aztec, Oxford Instruments Pty. Ltd) was used for elemental analysis at an accelerating voltage of 20 kV.

Cytotoxicity assay. To investigate cell cytotoxicity of the PAuNPs-MCs, a methyl thiazolyl tetrazolium (MTT) assay was applied. L929 cells were seeded at 2 x 10^5 cells/well into individual wells of 2 x 24-well culture trays in minimum essential medium (MEM) supplemented with 10% (v/v) fetal bovine serum (FBS) and 1% (v/v) non-essential amino acids (NEAA) as previously reported.[61]

Stability test. Mechanical stability of MCs was assessed by shaking the MCs (about 100 MCs) in 0.9 w/v% saline on an orbital mixer incubator (110 rpm) at 37 ºC. Microscopic observation (photographically recorded) and UV-Visible spectroscopy of the medium were used to evaluate the MCs integrity and detachment of AuNPs. In addition, identical analysis was performed on MCs before and after autoclaving.

Cadaver animal model studies. Following institutional guidelines for the use of laboratory animals, 15 weeks old mice and 3 weeks old weaner rats, used for other experiments were used at the Paul Scherrer Institute (PSI) animal facility and the Australian Synchrotron, respectively, and stored frozen. Cadavers were defrosted and were injected with a total of about 20 MCs in saline into the peritoneal cavity with a 14-gauge catheter while in a lateral position. The catheter was removed and the injection hole was pressed close for about 2 min to prevent MCs leakage. After transplantation of the MCs, the cadavers were used for imaging in the subsequent 30 minutes for small animal CT measurement (at PSI animal facility) or were fixed in 10% formalin (5 times the sample volume) before being transferred to smaller containers for the synchrotron CT measurements.

X-ray imaging. X-ray imaging of *in vitro* MCs and *post-mortem* animals injected with MCs was conducted at the Imaging and Medical Beamline at the Australian Synchrotron[62] (Clayton, Victoria, Australia) for quantitative analysis. The linear attenuation property of the MCs was determined using monochromatic X-ray beam at 25keV. The MCs were placed in 0.6 mL cone tubes (Eppendorf) and kept in saline solution to keep the samples from drying out. A total of 1800 projections were acquired over 180 degrees in continuous mode with exposure times of 200 ms at 25 keV. The X-rays were converted into visible light by a Gadolinium scintillator 25 µm thick. The detector used was a pco.edge CMOS camera (pco.edge, PCO AG, Kelheim, Germany) coupled with a lens system that permits to vary the pixel size continuously.[63] The data were acquired using an effective pixel size of 10 µm and an X-ray beam size of 25 × 5.2 mm^2. The slices reconstructions were performed using X-TRACT software (www.ts-imaging.net). For *post-mortem* animals at low X-ray dose a Scint-X DXI-11000 CCD camera coupled with a structured CsI scintillator 225 µm thick that provides higher conversion efficiency was used. The X-ray entrance dose for each CT scan was 75 mGy at 35 keV and it was measured and monitored during the CT acquisition using an ionization chamber in air. The images were captured using a pixel re-binning factor of 6 that provides an effective pixel size of 54 µm. The X-ray beam was 36 × 4.8 mm^2. A total of 1440 projections with an exposure time of 35 ms were acquired over 360 degrees illuminating half of the sample. The slices reconstructions were performed using the software PITRE[64] applying a subset of the acquired projection to evaluate the effect of number of projections/X-ray dose reduction on the image quality. The injected mice were

imaged using the NanoSPECT/CT Bioscan available at PSI. The CT setting was 45 kVp and 177 µA. A total of 180 projections were acquired over 180 degrees with an exposure time of 500 ms resulting in a computed tomography dose index (CTDI) of 28 mGy. The X-ray dose was intentionally kept low to test the MCs visibility in a critical situation since the capability to segment the MCs decrease with low X-ray dose.[42] The 3D rendering shown in Fig. 6 was prepared using the open source software Drishti v2.4 developed by Ajay Limaye. To improve the rendering result we segmented the MCs area in a separate volume and we merged it subsequently with the rest of the sample. In this way we could enhance the MCs signal independently from the bones and soft tissues signals.

Conclusions

This study has demonstrated a simple and novel fabrication method of gold coated alginate MCs that enable effective X-ray imaging in a *post-mortem* animal model. The imaging contrast agents developed for this study have several advantages when compared with MRI imaging contrast agents, including the ease of preparation, reduced cost of imaging technique, and faster acquisition time. The resulting labeled MCs exhibited low cytotoxicity and high mechanical stability *in vitro*. The novel fabrication method reported here results in a higher localized Au concentration which significantly increases the X-ray attenuation coefficient and thus results in a higher contrast compared to equivalent Au blended MCs. Most importantly, in contrast to earlier reports, the imaging of the gold coated MCs results in a very distinctive ring around the MCs enabling them to be readily distinguished from natural artefacts. Moreover, due to their high linear attenuation coefficient resulted from having a high Au loading and high localized concentration, the labeled MCs were compatible with longitudinal tracking studies since effective imaging can be achieved using a fast scan at low X-ray doses required for imaging at multiple time points.. With increasing use of MCs in drug delivery and cell therapies, the novel protocol for fabrication of AuNPs into a coating around MCs described here is a promising approach to enable the *in vivo* tracking of the MCs over time.

Acknowledgements

The authors thank the China Scholarship Council (CSC) and CSIRO for the financial support to the first author; Dani Cardozo (CSIRO) for supplying post-mortem animals; Vijay Vaithilingam (CSIRO) for assistance with the preparation of MCs; Lynne J. Waddington for SEM characterization (CSIRO); Fei Huang (CSIRO) for help with polymer synthesis; and Dr Shanmei Wang (Tongji University, China) with implantation of MCs. The authors also thank the Australian Synchrotron staff of Imaging and Medical Beamline for their help with imaging experiments.

Notes and references

[a] Beijing Key Lab of Bioprocess, Beijing University of Chemical Technology, Beijing, PR China
[b] Manufacturing Flagship, CSIRO, Clayton, VIC Australia
[c] Swiss Light Source, Paul Scherrer Institute, Villigen, Switzerland
[d] Australian Synchrotron, 800 Blackburn Rd, Clayton, VIC Australia
[e.] Center for Radiopharmaceutical Sciences ETH-PSI-USZ, Paul Scherrer Institute, Villigen, Switzerland
[f.] Manufacturing Flagship, CSIRO, North Ryde, NSW Australia

Electronic Supplementary Information (ESI) available: (including NMR spectra and TGA chromatogram of polymers, SEM imaging, EDS analysis, UV-Visible spectra of MCs and CT images of unlabeled MCs). See DOI: 10.1039/b000000x/

1. K. Y. Lee and D. J. Mooney, *Prog. Polym. Sci.*, 2012, **37**, 106-126.
2. J. S. Boateng, K. H. Matthews, H. N. Stevens and G. M. Eccleston, *J. Pharm. Sci.*, 2008, **97**, 2892-2923.
3. S. Maiti, K. Singha, S. Ray, P. Dey and B. Sa, *Pharm. Dev. Technol.*, 2009, **14**, 461-470.
4. K. H. Bouhadir, E. Alsberg and D. J. Mooney, *Biomaterials*, 2001, **22**, 2625-2633.
5. R. A. Ishak, G. A. Awad, N. D. Mortada and S. A. Nour, *J. Controlled Release*, 2007, **119**, 207-214.
6. K. Y. Lee, M. C. Peters and D. J. Mooney, *J. Controlled Release*, 2003, **87**, 49-56.
7. E. A. Silva and D. J. Mooney, *Biomaterials*, 2010, **31**, 1235-1241.
8. A. W. Chan and R. J. Neufeld, *Biomaterials*, 2010, **31**, 9040-9047.
9. P. Soon-Shiong, E. Feldman, R. Nelson, R. Heintz, Q. Yao, Z. Yao, T. Zheng, N. Merideth, G. Skjak-Braek and T. Espevik, *Proc. Natl. Acad. Sci.*, 1993, **90**, 5843-5847.
10. E. A. Ryan, B. W. Paty, P. A. Senior, D. Bigam, E. Alfadhli, N. M. Kneteman, J. R. Lakey and A. J. Shapiro, *Diabetes*, 2005, **54**, 2060-2069.
11. A. J. Shapiro, J. R. Lakey, E. A. Ryan, G. S. Korbutt, E. Toth, G. L. Warnock, N. M. Kneteman and R. V. Rajotte, *N. Engl. J. Med.*, 2000, **343**, 230-238.
12. A. Ault, *Lancet*, 2003, **361**, 2054.
13. M. Gotthardt, *Diabetes*, 2011, **60**, 381-382.
14. B. P. Barnett, A. Arepally, P. V. Karmarkar, D. Qian, W. D. Gilson, P. Walczak, V. Howland, L. Lawler, C. Lauzon and M. Stuber, *Nat. Med.*, 2007, **13**, 986-991.
15. G. Mai, N. T. Huy, P. Morel, J. Mei, A. Andres, D. Bosco, R. Baertschiger, C. Toso, T. Berney and P. Majno, *Xenotransplantation*, 2005, **12**, 457-464.
16. F. Lim and A. M. Sun, *Science (New York, NY)*, 1980, **210**, 908.
17. Y. Teramura and H. Iwata, *Adv. Drug Delivery Rev.*, 2010, **62**, 827-840.
18. H. Zimmermann, S. G. Shirley and U. Zimmermann, *Curr. Diabetes Rep.*, 2007, **7**, 314-320.
19. B. E. Tuch, G. W. Keogh, L. J. Williams, W. Wu, J. L. Foster, V. Vaithilingam and R. Philips, *Diabetes Care*, 2009, **32**, 1887-1889.
20. B. E. Tuch, T. C. Hughes and M. D. Evans, *Diabetes-Metab Res. Rev.*, 2011, **27**, 928-932.
21. D. A. Kedziorek, L. V. Hofmann, Y. Fu, W. D. Gilson, K. M. Cosby, B. Kohl, B. P. Barnett, B. W. Simons, P. Walczak and J. W. Bulte, *Stem Cells*, 2012, **30**, 1286-1296.
22. B. Barnett, D. Kraitchman, C. Lauzon, C. Magee, P. Walczak, W. Gilson, A. Arepally and J. Bulte, *Mol Pharmaceutics*, 2006, **3**, 531-538.
23. D. R. Arifin, S. Manek, E. Call, A. Arepally and J. W. Bulte, *Biomaterials*, 2012, **33**, 4681-4689.
24. D. R. Arifin, C. M. Long, A. A. Gilad, C. Alric, S. Roux, O. Tillement, T. W. Link, A. Arepally and J. W. Bulte, *Radiology*, 2011, **260**, 790-798.
25. J. Kim, D. R. Arifin, N. Muja, T. Kim, A. A. Gilad, H. Kim, A. Arepally, T. Hyeon and J. W. Bulte, *Angew. Chem. Int. Ed.*, 2011, **123**, 2365-2369.
26. T. W. Link, D. Woodrum, W. D. Gilson, L. Pan, D. Qian, D. L. Kraitchman, J. W. Bulte, A. Arepally and C. R. Weiss, *J. Vasc. Interv. Radiol.*, 2011, **22**, 1335-1340.
27. P. H. Mills, T. K. Hitchens, L. M. Foley, T. Link, Q. Ye, C. R. Weiss, J. D. Thompson, W. D. Gilson, A. Arepally and J. A. Melick, *Magn. Reson. Med.*, 2012, **67**, 278-289.

28. T. W. Link, D. R. Arifin, C. M. Long, P. Walczak, N. Muja, A. Arepally and J. W. Bulte, *Cell Med.*, 2012, **4**, 77.
29. B. P. Barnett, J. Ruiz-Cabello, P. Hota, R. Liddell, P. Walczak, V. Howland, V. P. Chacko, D. L. Kraitchman, A. Arepally and J. W. Bulte, *Radiology*, 2011, **258**, 182-191.
30. J. H. Hubbell and S. M. Seltzer, *National Institute of Standards and Technology*, 5632, Web version 1.02, **1997**. Available at: http://www.physics.nist.gov/PhysRefData/XrayMassCoef/cover.html. Accessed October 12, 1999.
31. R. A. Sperling, P. R. Gil, F. Zhang, M. Zanella and W. J. Parak, *Chem. Soc. Rev.*, 2008, **37**, 1896-1908.
32. P. K. Jain, K. S. Lee, I. H. El-Sayed and M. A. El-Sayed, *J. Phys. Chem. B*, 2006, **110**, 7238-7248.
33. D. Xi, S. Dong, X. Meng, Q. Lu, L. Meng and J. Ye, *RSC Adv.*, 2012, **2**, 12515-12524.
34. R. H. Menk, E. Schültke, C. Hall, F. Arfelli, A. Astolfo, L. Rigon, A. Round, K. Ataelmannan, S. R. MacDonald and B. H. Juurlink, *Nanomed-Nanotechnol.*, 2011, **7**, 647-654.
35. A. Astolfo, E. Schültke, R. H. Menk, R. D. Kirch, B. H. Juurlink, C. Hall, L.-A. Harsan, M. Stebel, D. Barbetta and G. Tromba, *Nanomed-Nanotechnol.*, 2013, **9**, 284-292.
36. A. Astolfo, F. Arfelli, E. Schultke, S. James, L. Mancini and R.-H. Menk, *Nanoscale*, 2013, **5**, 3337-3345.
37. H. Wang, L. Zheng, C. Peng, R. Guo, M. Shen, X. Shi and G. Zhang, *Biomaterials*, 2011, **32**, 2979-2988.
38. C. Peng, L. Zheng, Q. Chen, M. Shen, R. Guo, H. Wang, X. Cao, G. Zhang and X. Shi, *Biomaterials*, 2012, **33**, 1107-1119.
39. S. Ahn, S. Y. Jung, E. Seo and S. J. Lee, *Biomaterials*, 2011, **32**, 7191-7199.
40. B. P. Barnett, A. Arepally, M. Stuber, D. R. Arifin, D. L. Kraitchman and J. W. Bulte, *Nat. Protoc.*, 2011, **6**, 1142-1151.
41. D. R. Arifin, C. M. Long, A. A. Gilad, C. Alric, S. Roux, O. Tillement, T. W. Link, A. Arepally and J. W. M. Bulte, *Radiology*, **260**, 790-798.
42. A. Astolfo, F. Qie, A. Kibleur, X. Hao, R. H. Menk, F. Arfelli, L. Rigon, T. M. Hinton, M. Wickramaratna and T. Tan, *Nanomed-Nanotechnol.*, 2014, **10**, 1821-1828.
43. C. Wang, X. Wang, S. W. Anderson and X. Zhang, *Sens. Actuators B*, 2014, **196**, 670-675.
44. Y. Li, J. Wang, C. Holloway and D. B. Plewes, *Phys. Med. Bio.*, 2005, **50**, 3349.
45. Q.-L. Fan, K.-G. Neoh, E.-T. Kang, B. Shuter and S.-C. Wang, *Biomaterials*, 2007, **28**, 5426-5436.
46. F. Hu, K. G. Neoh, L. Cen and E.-T. Kang, *Biomacromolecules*, 2006, **7**, 809-816.
47. M. Brust, M. Walker, D. Bethell, D. J. Schiffrin and R. Whyman, *J. Chem. Soc., Chem. Commun.*, 1994, 801-802.
48. J. S. Kim, H. J. Jeon, J. J. Park, M. S. Park and J. H. Youk, *J. Polym. Sci. Pol. Chem.*, 2009, **47**, 4963-4970.
49. G. Chen, P. M. Wright, J. Geng, G. Mantovani and D. M. Haddleton, *Chem. Commun.*, 2008, 1097-1099.
50. G. Frens, *Nature*, 1973, **241**, 20-22.
51. W. Haiss, N. T. Thanh, J. Aveyard and D. G. Fernig, *Anal. Chem.*, 2007, **79**, 4215-4221.
52. R. Elghanian, J. J. Storhoff, R. C. Mucic, R. L. Letsinger and C. A. Mirkin, *Science*, 1997, **277**, 1078-1081.
53. C. Boyer, A. Bousquet, J. Rondolo, M. R. Whittaker, M. H. Stenzel and T. P. Davis, *Macromolecules*, 2010, **43**, 3775-3784.
54. A.-S. Duwez, P. Guillet, C. Colard, J.-F. Gohy and C.-A. Fustin, *Macromolecules*, 2006, **39**, 2729-2731.
55. C.-A. Fustin and A.-S. Duwez, *J. Electron. Spectrosc.*, 2009, **172**, 104-106.
56. Y. Liu, T. C. Hughes, B. W. Muir, L. J. Waddington, T. R. Gengenbach, C. D. Easton, T. M. Hinton, B. A. Moffat, X. Hao and J. Qiu, *Biomaterials*, 2014, **35**, 378-386.
57. C. Boyer, M. R. Whittaker, C. Nouvel and T. P. Davis, *Macromolecules*, 2010, **43**, 1792-1799.
58. D. Pissuwan, C. Boyer, K. Gunasekaran, T. P. Davis and V. Bulmus, *Biomacromolecules*, 2010, **11**, 412-420.
59. http://physics.nist.gov/PhysRefData/XrayMassCoef/cover.html via XMuDat software developed by R. Nowotny.
60. Y. Liu, X. Hao, L. Waddington, J. Qiu and T. Hughes, *Aust. J. Chem.*, 2013, **67**, 151-158.
61. M. D. Evans, R. K. Prakasam, P. K. Vaddavalli, T. C. Hughes, W. Knower, J. S. Wilkie, K. M. McLean, G. Johnson, G. A. McFarland and R. Z. Xie, *Biomaterials*, 2011, **32**, 3158-3165.
62. A. W. Stevenson, C. J. Hall, S. C. Mayo, D. Hausermann, A. Maksimenko, T. E. Gureyev, Y. I. Nesterets, S. W. Wilkins and R. A. Lewis, *J. Synchrotron Rad.*, 2012, **19**, 728-750.
63. C. Hall, D. Hausermann, A. Maksimenko, A. Astolfo, K. Siu, J. Pearson and A. Stevenson, *J. Instrum.*, 2013, **8**, C06011.
64. R.-C. Chen, D. Dreossi, L. Mancini, R. Menk, L. Rigon, T.-Q. Xiao and R. Longo, *J. Synchrotron Rad.*, 2012, **19**, 836-845.

